Arctic shrub effects on NDVI, summer albedo and soil shading

Juszak, Inge ; Erb, Angela M ; Maximov, Trofim C ; Schaepman-Strub, Gabriela

Abstract: The influence of Arctic vegetation on albedo, latent and sensible heat fluxes, and active layer thickness is a crucial link between boundary layer climate and permafrost in the context of climate change. Shrubs have been observed to lower the albedo as compared to lichen or graminoid-tundra. Despite its importance, the quantification of the effect of shrubification on summer albedo has not been addressed in much detail. We manipulated shrub density and height in an Arctic dwarf birch (Betula nana) shrub canopy to test the effect on shortwave radiative fluxes and on the normalized difference vegetation index (NDVI), a proxy for vegetation productivity used in satellite-based studies. Additionally, we parametrised and validated the 3D radiative transfer model DART to simulate the amount of solar radiation reflected and transmitted by an Arctic shrub canopy. We compared results of model runs of different complexities to measured data from North-East Siberia. We achieved comparably good results with simple turbid medium approaches, including both leaf and branch optical property media, and detailed object based model parameterisations. It was important to explicitly parameterise branches as they accounted for up to 71% of the total canopy absorption and thus contributed significantly to soil shading. Increasing leaf biomass resulted in a significant increase of the NDVI, decrease of transmitted photosynthetically active radiation, and repartitioning of the absorption of shortwave radiation by the canopy components. However, experimental and modelling results show that canopy broadband nadir reflectance and albedo are not significantly decreasing with increasing shrub biomass. We conclude that the leaf to branch ratio, canopy background, and vegetation type replaced by shrubs need to be considered when predicting feedbacks of shrubification to summer albedo, permafrost thaw, and climate warming.

DOI: https://doi.org/10.1016/j.rse.2014.07.021

Arctic shrub effects on NDVI, summer albedo and soil shading

Inge Juszak[a], Angela M. Erb[a,b], Trofim C. Maximov[c], Gabriela Schaepman-Strub[a]

[a] *Institute of Evolutionary Biology and Environmental Studies, University of Zurich, Winterthurerstrasse 190, 8057 Zurich, Switzerland*
[b] *now at: School for the Environment, University of Massachusetts Boston, 100 Morrisey Boulevard, Boston, MA 02125-3393, USA*
[c] *Biological Problems of the Cryolithozone, Russian Academy of Sciences, Siberian Division, 41 Lenin Prospekt, Yakutsk, Yakutia 677980, Russian Federation*

Abstract

The influence of Arctic vegetation on albedo, latent and sensible heat fluxes, and active layer thickness is a crucial link between boundary layer climate and permafrost in the context of climate change. Shrubs have been observed to lower the albedo as compared to lichen or graminoid-tundra. Despite its importance, the quantification of the effect of shrubification on summer albedo has not been addressed in much detail. We manipulated shrub density and height in an Arctic dwarf birch (*Betula nana*) shrub canopy to test the effect on shortwave radiative fluxes and on the normalized difference vegetation index (NDVI), a proxy for vegetation productivity used in satellite-based studies. Additionally, we parametrised and validated the 3D radiative transfer model DART to simulate the amount of solar radiation reflected and transmitted by an Arctic shrub canopy. We compared results of model runs of different complexities to measured data from North-East Siberia. We achieved comparably good results with simple turbid medium approaches, including both leaf and branch optical property media, and detailed object based model parameterisations. It was important to explicitly parameterise branches as they accounted for up to 71% of the total canopy absorption and thus contributed significantly to soil shading. Increasing

*Corresponding author
Email address: inge.juszak@ieu.uzh.ch, +41446354839 (Inge Juszak)

leaf biomass resulted in a significant increase of the NDVI, decrease of transmitted photosynthetically active radiation, and repartitioning of the absorption of shortwave radiation by the canopy components. However, experimental and modelling results show that canopy broadband nadir reflectance and albedo are not significantly decreasing with increasing shrub biomass. We conclude that the leaf to branch ratio, canopy background, and vegetation type replaced by shrubs need to be considered when predicting feedbacks of shrubification to summer albedo, permafrost thaw, and climate warming.

Keywords: 3D radiative transfer modelling; Manipulation experiment; Arctic shrubs; Shortwave radiation balance; NDVI; Albedo; tPAR; Branch to leaf ratio

1. Introduction

Arctic ecosystems have been exposed to air temperature increases of almost double the global mean in the 20th century (Chapin III et al., 2000; Serreze et al., 2000; Solomon et al., 2007; Cowtan & Way, 2014). Further increases in air temperature and precipitation, as projected for the north-eastern Siberian tundra (Solomon et al., 2007), may cause further shifts in the vegetation distribution in the Arctic (Pearson et al., 2013). Currently observed changes include northward movement of trees and shrubs, which increasingly dominate large areas of tundra (e.g. Sturm et al., 2001; Tape et al., 2006; Myers-Smith et al., 2011; Miller & Smith, 2012). Productivity estimates based on remote sensing, dendroecological, and plot data show an increasing trend with temperature, while the sensitivity of this effect is mediated by soil moisture, with productivity in wet areas responding stronger to temperature increase than in dry areas (Forbes et al., 2010; Huemmrich et al., 2010; Blok et al., 2011b; Elmendorf et al., 2012; Berner et al., 2013; Kim et al., 2014).

Shrub cover and distribution is not only affected by climate, it also controls important components of the surface energy balance. Main observed and expected feedbacks of increasing shrub cover include a reduction of the albedo,

an increase in evapotranspiration, and a local decrease in the permafrost active layer due to soil shading (Pearson et al., 2013). Shrub cover reduces the surface albedo during the growing season (Beringer et al., 2005; Sturm et al., 2005; Bonfils et al., 2012), but the effect is most pronounced during critical snow accumulation and snowmelt periods (Sturm et al., 2005; Loranty et al., 2011). The additional shortwave radiation absorbed by the canopy is partly partitioned into latent and sensible heat fluxes which are likely to increase with increasing shrub height and density (Beringer et al., 2005; Bonfils et al., 2012). Increasing shrub cover increases surface roughness and thus the coupling between the atmosphere and the surface (Beringer et al., 2005). These fluxes are also modulated by other system properties including soil moisture and the presence of mosses (Blok et al., 2011a).

Additionally, shrubs affect the amount of shortwave radiation transmitted to the soil surface, an important component of the soil surface energy balance (Eugster et al., 2000). While shrubs increased the winter soil temperature, summer soil temperature was reduced through shading (Myers-Smith & Hik, 2013). At least at the local scale, shrub shading may offset air temperature warming and reduce active layer thickness (Blok et al., 2010; Jorgenson et al., 2010). These changes in the energy balance resulting from shrub expansion may in turn facilitate further shrub growth (Chapin III et al., 2005; Swann et al., 2010).

The quantification of the effect of shrubification on summer albedo has not been addressed in much detail, apart from observations across a latitudinal gradient. It is hard to relate satellite based albedo data to shrub abundance in the Arctic as the spatial resolution of operational satellite-derived albedo products is 0.5-1 km. As such, we are currently unable to effectively assess shrub cover and abundance at this scale. We therefore performed an experimental and radiative transfer modelling study to disentangle the effect of shrub density and height on reflected and transmitted shortwave radiation fluxes and NDVI, the proxy most often used to estimate long-term productivity at large spatial scale (e.g. Hope et al., 2004; Bhatt et al., 2010). Radiative transfer modelling can help to quantify reflected and transmitted shortwave radiation, including sub-

daily and seasonal variation (Widlowski et al., 2011). It can be used to validate simpler approaches which are often used in large-scale modelling (Pinty et al., 2006). Two studies on Arctic shrubs quantify the absorption of solar radiation of woody elements before leaf-out (Bewley et al., 2007; Reid et al., 2014), but, to our knowledge, no study so far has simulated the full radiative budget of Arctic dwarf shrub leaves and branches including spectral reflectance of the canopy and transmitted radiation.

We present results of modelling and experimental work on the effect of dwarf birch leaf and branch area on the radiative balance. Unlike most studies on the effect of vegetation on the energy balance of the Arctic (e.g. Beringer et al., 2005; Chapin III et al., 2005; Loranty et al., 2011), we did not compare different ecosystems but quantified the effects of varying biomass within one vegetation type. We ran the 3D radiative transfer model DART (Gastellu-Etchegorry et al., 1996; Grau & Gastellu-Etchegorry, 2013) for shrub vegetation of different densities. The model was initialised with field data which included detailed information on vegetation structure and leaf and branch optical properties. We validated the model with canopy reflected and transmitted radiation measurements on natural canopies and vegetation with experimentally reduced density. We compared results from models with different levels of complexity to assess the importance of detailed shrub representation on shortwave radiation results.

2. Methods

2.1. Field site

The Kytalyk field site is located in the Indigirka lowlands, North-East Siberia (70.83 °N, 147.49 °E, Figure 1, a). The mean annual air temperature is −10.5 °C with a range of −32.5 °C in January and 10.4 °C in July (van der Molen et al., 2007). The mean annual precipitation is 220 mm (Parmentier et al., 2011). Kytalyk is in the continuous permafrost zone with an average active-layer thickness (ALT) of 42 cm. Dry areas show a reduced ALT of 12-28 cm, while the ALT in wetter areas ranges from 22-50 cm (Mi et al., 2013).

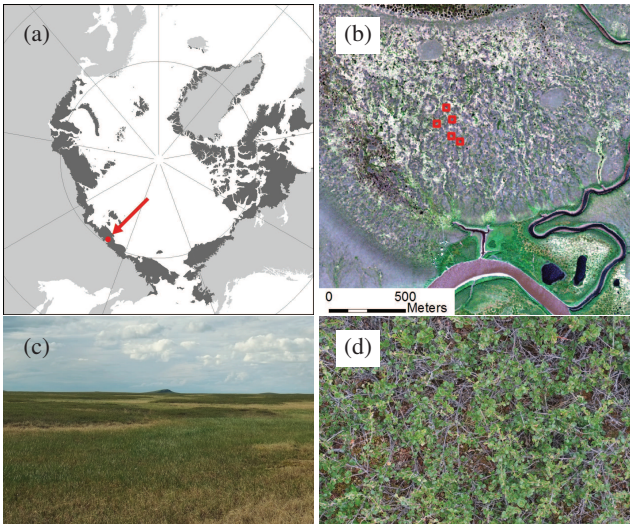

Figure 1: Overview of the stations location in north-east Siberia and the extent of Arctic tundra (a, dark grey, data from Walker et al. (2005)), satellite image (GeoEye-1) of the site with the location of the five plots (b, red squares), tundra landscape (c) and dwarf birch vegetation (d, detail of about 60·90 cm).

The Circumpolar Arctic Vegetation Map classifies the vegetation at the study site as tussock-sedge, dwarf-shrub, moss tundra (Walker et al., 2005). Dwarf birch (*Betula nana*) is the main shrub type (Figure 1, d). Shrubs and sedges are arranged alternately in small patches associated with micro topography and moisture on the scale of a few meters in the area of a drained thaw lake bed (Figure 1, b and c).

2.2. Field experiment and measurements

We conducted a field campaign in June and July 2012 and measured input and validation data to parameterise a radiative transfer model for dwarf birch canopies. We performed a manipulation experiment to increase the variability and range of plot characteristics. The experiment included five replicate plots on different dwarf birch patches, each with a control, height, and density treatment. For the height treatment we removed the top 5 cm of all dwarf birch branches. For the density treatment we removed roughly one third of

the dwarf birch branches above the moss layer. We use the term 'branch' for dwarf birch ramets, separate units that belong to a clonal population. The branches, or ramets, are not connected above-ground and have simple shapes with minimal off-shoots. Additionally, subplots of complete shrub removal were used for background optical properties and biomass estimations. The control, height, and density treatment plots were $2\,\mathrm{m} \cdot 2\,\mathrm{m}$ in size and the removal plots were $0.8\,\mathrm{m} \cdot 0.8\,\mathrm{m}$. The vegetation characteristics after treatment are shown in Table 2. We tested all variables of interest for preexisting biases due to plot selection and evaluated the treatment effects over time with statistical methods.

Detailed information on vegetation structure and properties were required to parameterise the radiative transfer model. For the dwarf birch canopy we used point-quadrat grids to measure the leaf area index (LAI in $\mathrm{m}^2\,\mathrm{m}^{-2}$) and the branch area index (BAI in $\mathrm{m}^2\,\mathrm{m}^{-2}$) as well as the canopy height at three timepoints in June and July on each subplot (dates in Table 1). We recorded all leaf and branch hits on a $0.5\,\mathrm{m} \cdot 0.5\,\mathrm{m}$ grid of 81 points. Plant area index (PAI in $\mathrm{m}^2\,\mathrm{m}^{-2}$) is the sum of LAI and BAI. We use LAI as abbreviation for total, one-sided leaf area per ground area. As branches are cylindrical, we use the product of branch diameter and branch length as proxy for branch area. We counted the number of shrub stems and leaves and estimated the shape of a typical branch from photographs and measurements from a removed branch. The 3D branch structure was then reconstructed using the graphics software blender$^{\mathrm{TM}}$.

Additionally we measured leaf and bark optical properties (Figure 2) with an ASD spectrometer (Analytical Spectral Devices, Fieldspec4), high-intensity contact probe, and leaf clip. The ASD covers the spectral range of 350-2500 nm in 3 nm spectral resolution in the visible range and 10 nm spectral resolution in the NIR. We measured leaf top, leaf bottom, and bark spectral reflectance on a black background with a measurement spot size of 10 mm. We distinguished two types of dwarf birch branches, old branches with a grey colour (63% of the branches) and young branches, reddish in colour (37%). As we could not measure leaf transmittance (T) in the field, it was estimated from the measured leaf

reflectance (R) and two other datasets which included reflectance and transmittance using equation 1.

$$T_{estimated}(\lambda) = \max\left(R_{measured}(\lambda) \cdot \left(\frac{T_{reference}(\lambda)}{R_{reference}(\lambda)}\right), 0\right) \quad (1)$$

In the range λ =400-1900 nm we took the reference data from integrating sphere measurements of a horticultural dwarf birch in Zurich. For the longer wavelengths (1900-2500 nm), the integrating sphere data was too noisy so we used data for the silver birch (*Betula pendula*) from the LOPEX database (Hosgood et al., 1995, revised 2005) as a reference. This approach was used because, apart from the noise, the the ratio $\frac{T(\lambda)}{R(\lambda)}$ was similar for both reference data sets.

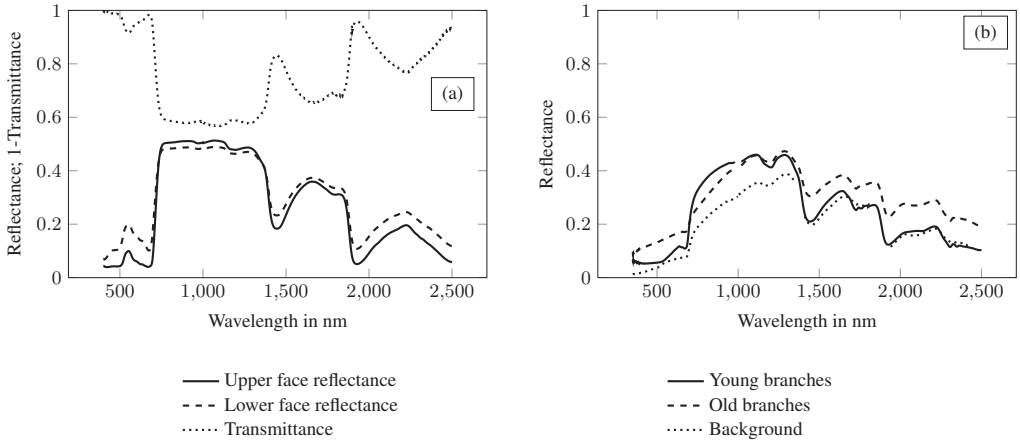

Figure 2: Mean dwarf birch leaf (a) and bark optical properties and background reflectance (b).

We used reflectance measurements of the removal plots as background property in the DART simulations (Figure 2, b). The background below the shrubs on average consisted of 50% dwarf birch litter, 48% mosses and 2% lichen.

Table 1: Details on all measured variables and the model inputs; * indicates measurements on plot 5 only.

Variable	Method	Dates in 2012	Value
Measured model input			
Leaf area index of dwarf birch (LAI)	Point-quadrant grid	18 - 19/06, 23/06* & 25/06 & 14/07	
Branch area index of dwarf birch (BAI)	Point-quadrant grid	18 - 19/06, 23/06* & 25/06 & 14/07	
Canopy height	Point-quadrant grid	06/07	23 cm±5 cm
Number of dwarf birch stems	Count on removal plots	29/06 - 04/07	
Number of dwarf birch leaves	Count on removal plots	21 - 23/06	
Dwarf birch branch structure	Manual measurements, photos, 3D model using blender^{TM}	20 - 23/06 & 29/06 & 04/07 & 06/07	Branch length ≈ 41 cm, leaf diameter ≈ 1 cm
Leaf spectral reflectance	ASD (contact probe)	14/07	
Branch spectral reflectance	ASD (contact probe)	05/07	
Background reflectance	ASD (nadir, 1 m, 5° field of view)	08/07	
Measured model validation			
tPAR	Delta T SunScan	18/06, 23/06* & 28/06 & 03/07	
Canopy reflectance	ASD (nadir, 1 m, 5° field of view)	18/06, 23/06* & 08/07 & 11/07	
Irradiance	ASD (white panel)	18/06, 23/06* & 08/07 & 11/07	
Other input parameters			
Sun zenith angle	Geometric	30/06, 1 h from solar noon	49°
Atmosphere parameterisation	DART sub-arctic winter, aerosols rural (V=23 km), aerosol optical depth factor: 0.2	Validated with measured irradiance	Aerosol optical depth at 550 nm: 0.065
Leaf angle distribution (for turbid medium)	Estimated (photos)		Spherical
Branch angle distribution (for turbid medium)	Estimated (photos)		Erectophile
General model set-up			
Mode			Flux tracking
Scene size			0.5 m · 0.5 m
Cell size			2.5 cm
Wavelength range			400-2500 nm
Wavelength interval			10 nm

To validate the radiative transfer model we measured canopy hemispherical-directional spectral reflected radiation (λ =350-2500 nm) vertically ≈1 m above the soil surface using an ASD with a 5° field of view. 25 single exitance readings were averaged for each measurement and we took three such measurements on every subplot at each time point. We measured spectral irradiance from the reflectance of a spectralon® white panel. From exitance and irradiance we calculated spectral reflectance (R_{nadir}, Equation 2) and broadband reflectance (Rb_{nadir}, Equation 3).

Furthermore we calculated the NDVI (Normalized Difference Vegetation Index), which is often used as a proxy for vegetation productivity (e.g. Beck & Goetz, 2011; Gamon et al., 2013). We calculated NDVI from the nadir spectral reflectance measurements using the red and NIR bands according to AVHRR (Advanced Very High Resolution Radiometer) specifications (Equation 4) as AVHRR data are often used in studies of Arctic vegetation (e.g. Hope et al., 2004; Bhatt et al., 2010).

$$R_{nadir}(\lambda) = \frac{\text{Exitance}(\lambda)}{\text{Irradiance}(\lambda)} \quad (2)$$

$$Rb_{nadir} = \frac{\sum_{\lambda=400\,\text{nm}}^{2500\,\text{nm}} \text{Exitance}(\lambda)}{\sum_{\lambda=400\,\text{nm}}^{2500\,\text{nm}} \text{Irradiance}(\lambda)} \quad (3)$$

$$\text{NDVI} = \frac{R_{nadir}(nir_{725-1000\,\text{nm}}) - R_{nadir}(red_{580-680\,\text{nm}})}{R_{nadir}(nir_{725-1000\,\text{nm}}) + R_{nadir}(red_{580-680\,\text{nm}})} \quad (4)$$

The Photosynthetically Active Radiation transmitted below the canopy (tPAR, 400-700 nm) was measured with a Delta-T Devices SunScan Canopy Analysis System. The system consists of two instruments with simultaneous recording: the SunScan Probe (SS1) is a one-meter long wand with 64 equally spaced sensors which is inserted below the canopy to measure the amount of transmitted PAR. The Sunshine Sensor (BF3) is mounted above the canopy and measures total incoming PAR and diffuse incoming PAR.

2.3. Modelling

The simulations were performed with the DART (Discrete Anisotropic Radiative Transfer) model (Gastellu-Etchegorry et al., 1996, 2004; Grau & Gastellu-Etchegorry, 2013) version 5.4.6. (November 2013). DART enables 3D radiative transfer simulations through atmosphere and canopies in the wavelength range 0.3-120 µm. The general settings and all model inputs are summarized in Table 1. We parameterised the reflectance of soil and understory below the shrub layer with the mean reflectance spectra of the removal subplot measurements after the treatment (Figure 2). This background reflectance is assumed to be lambertian and the transmittance of the background was set to zero.

We used two representations of shrub canopy, voxels filled with turbid medium and objects composed of small triangular surfaces. Turbid medium calculations require inputs on vegetation height and leaf angles (Table 1). In the simulations with objects, leaves were arranged on the branches as observed on a sample branch. All branches were included in the scene at randomly generated azimuth and elevation angles and positions. Six model complexities (Figure 3) were tested:

I Turbid cells with the optical properties of leaves

II Two classes of turbid cells with optical properties of leaves or branches

III Branches as idealised vertical cones ('stems') and turbid cells with leaf optical properties

IV Branches as triangulated objects and turbid cells with leaf optical properties

V Branches and leaves as triangulated objects

VI Only leaves as triangulated objects

For all complexities we varied PAI between 0 and 4 in steps of 0.4. We used an equal contribution of leaves and branches assuming LAI = BAI = PAI/2, which agrees well with the point-quadrat measurements on control subplots

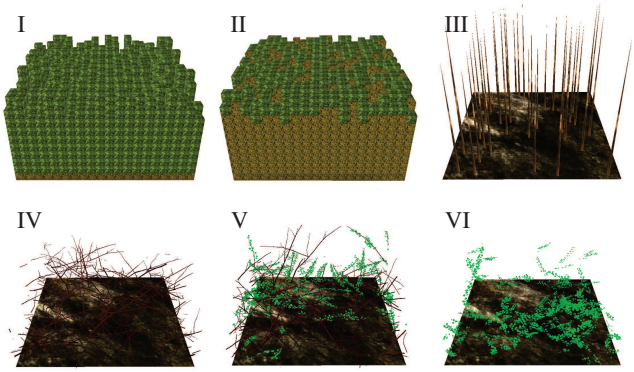

Figure 3: Visualisation of the six DART model complexities, each shown for LAI = BAI = 0.2; III and IV additionally contain leaves as turbid medium which would obstruct the branches in the visualisation.

(Figure 4 a, b; Table 2). For the complexities which include branches, we additionally simulated the scene with a constant PAI of 2 and different contributions of leaves and branches (LAI between 0 and 2 and corresponding BAI between 2 and 0 in steps of 0.2).

For model validation we used four outputs which correspond to our field data, tPAR, nadir spectral (R_{nadir}, Equation 2) and broadband (Rb_{nadir}, Equation 3) reflectance, and NDVI (Equation 4). Further model outputs that cannot be validated with our field data are other components of the 3D radiative budget including the fraction of transmitted, absorbed, and reflected radiation and the reflectance in directions other than nadir.

3. Results

3.1. Treatment effects on the dwarf shrub canopy

We assessed the treatment effect by testing LAI, BAI, tPAR, Rb_{nadir}, and NDVI for pre-treatment biases (Figure 4). Before treatment none of the five variables was significantly different between either density or height subplots and control subplots. After the treatment LAI, tPAR, and NDVI were significantly different on both density and height subplots as compared to control subplots

(Figure 4). The P-values of BAI and Rb_{nadir} were smaller after treatment than before treatment, however, the differences between treatment subplots and control subplots were not statistically significant (Figure 4). In all cases the location of the subplots was not significant ($P > 0.01$, values not shown).

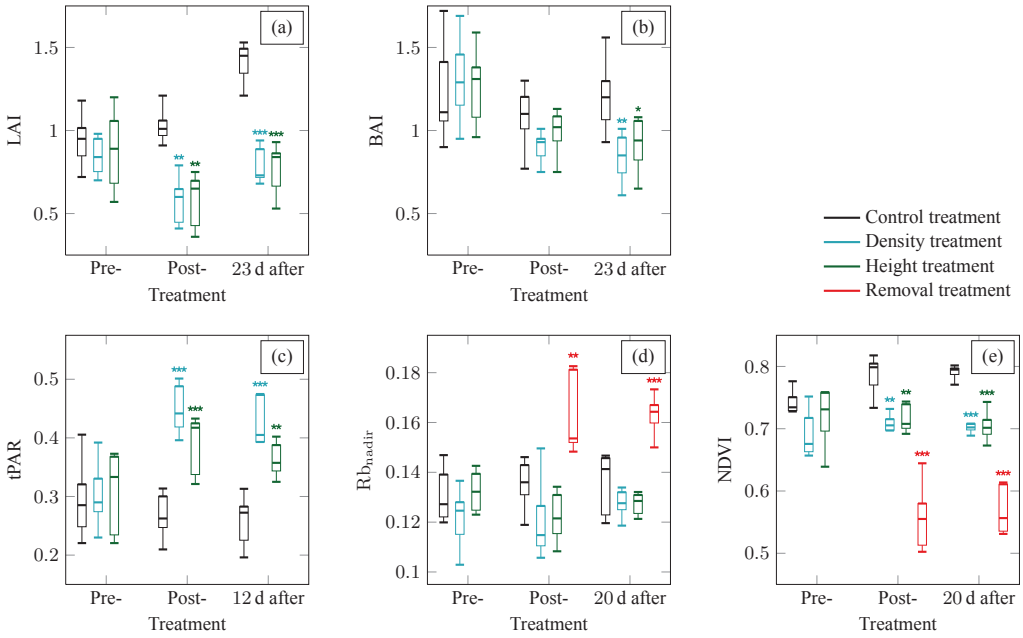

Figure 4: Effect of treatment and variation with time of LAI (a), BAI (b), tPAR (c), Rb_{nadir} (d), and NDVI (e); the central mark of the boxes is the median of five replicate plots, the edges are the 25th and 75th percentiles, and the whiskers denote the most extreme values; significance of the difference between control and other treatment subplots for each time step: $p < 0.001 :^{***}, p < 0.01 :^{**}, p < 0.05 :^{*}$; measurement dates in Table 1.

The magnitude and direction of the change induced by the treatments is shown in Table 2. As could be expected, tPAR increased on density and height subplots due to biomass removal. Broadband nadir reflectance (Rb_{nadir}) was lower on density and height subplots as compared to control subplots while the total shrub removal increased the reflectance. In general, reflectance showed small differences between the treatments and over time. This can be attributed to the weak correlation between the reflectance and LAI, BAI or PAI in the range of $1 < PAI < 3$ (Table 3). The biomass removal led to reduced NDVI

Table 2: Post-treatment measurements: mean and standard deviation of five replicate plots and mean difference between treatment and control subplots in percent of the control measurement; negative values show a reduction due to the treatment, positive values an increase.

	Control	Density		Height		Removal	
	Value	Value	Dif. (%)	Value	Dif. (%)	Value	Dif. (%)
Fresh biomass ($\mathrm{kg\,m^{-2}}$)	1.54 ± 0.33	1.09 ± 0.28	-28.9	1.36 ± 0.31	-11.4	-	
Canopy height (cm)	23.3 ± 2.3	20.9 ± 3.7	-10.4	16.6 ± 1.0	-28.7	-	
Branches per $\mathrm{m^2}$	107 ± 14	72 ± 11	-32.3	119 ± 20	11.5	-	
LAI	1.03 ± 0.11	0.57 ± 0.15	-44.2	0.58 ± 0.17	-43.7	-	
BAI	1.09 ± 0.20	0.90 ± 0.10	-17.1	0.99 ± 0.15	-8.5	-	
tPAR	0.27 ± 0.04	0.45 ± 0.04	67.7	0.39 ± 0.05	44.4	-	
$\mathrm{Rb_{nadir}}$	0.14 ± 0.01	0.12 ± 0.02	-11.3	0.12 ± 0.01	-9.8	0.16 ± 0.02	20.8
NDVI	0.79 ± 0.03	0.71 ± 0.01	-9.9	0.72 ± 0.02	-8.8	0.56 ± 0.06	-29.4

values (Table 2). We observed a notable increase over time in LAI and NDVI on control subplots between the pre- and post-treatment measurements, indicating vegetation development (Figure 4, a, e). The treatment also changed the leaf to branch ratio of the shrub vegetation. While LAI/BAI increased strongly over time in the control subplots, the treatment subplots only showed an increase over time between the last two measurements and the ratios were generally lower, especially for the height treatment.

3.2. tPAR - data and model results

The amount of transmitted radiation below the canopy (tPAR) decreases with increasing plant area (Figure 5, a). The correlation coefficient between measured tPAR and PAI is -0.79, which is stronger than the correlation of tPAR with LAI or BAI (-0.65 and -0.62, respectively; Table 3). Thus for tPAR both leaves and branches have to be considered.

All model simulations reproduce the observed decrease of tPAR with PAI (Figure 5, a). However, all model complexities also underestimate tPAR, especially those which include object branches or stems, which simulate values outside of the 95% confidence interval of the data (III-V, Figure 5, a). For the turbid medium approach the medium classification has a negligible influence on

Table 3: Pearson's correlation coefficients of LAI, BAI, and PAI with tPAR, nadir broadband reflectance (Rb_{nadir}), and NDVI for all measurements except removal subplots.

	tPAR	Rb_{nadir}	NDVI
LAI	-0.65	0.37	0.73
BAI	-0.62	-0.08	0.09
PAI	-0.79	0.19	0.53

tPAR as the reflectance of branches and leaves is similar in the visible range and leaf transmittance is only 7.7%.

The ratio between leaves and branches influences tPAR less than total PAI (Figure 5, b). For II (turbid leaves and turbid branches), tPAR is almost identical for all ratios between leaves and branches, whereas all other complexities show between 2.3 and 3.3 times higher tPAR for simulations with only leaves as compared to only branches (Figure 5, b).

3.3. Reflectance - data and model results

The measured broadband nadir reflectance varies only slightly between 0.1 and 0.15 (Figure 4, d) and is weakly related to PAI (correlation coefficient of 0.19, Table 3). The correlation with LAI is 0.37, slightly stronger. Thus we observe that the amount of plant material does not have a strong effect on reflectance and possibly has a weak positive effect in the range of 1-3 PAI.

Unlike with tPAR, the simulation complexities reveal substantial differences in the relationship between PAI and reflectance. I and VI, which only consider leaves, clearly overestimate the reflectance which in simulations increases strongly with PAI (Figure 5, c). Without branches the simulated reflectance is higher than the background reflectance (shown at PAI = 0), due in part to the relatively dark background.

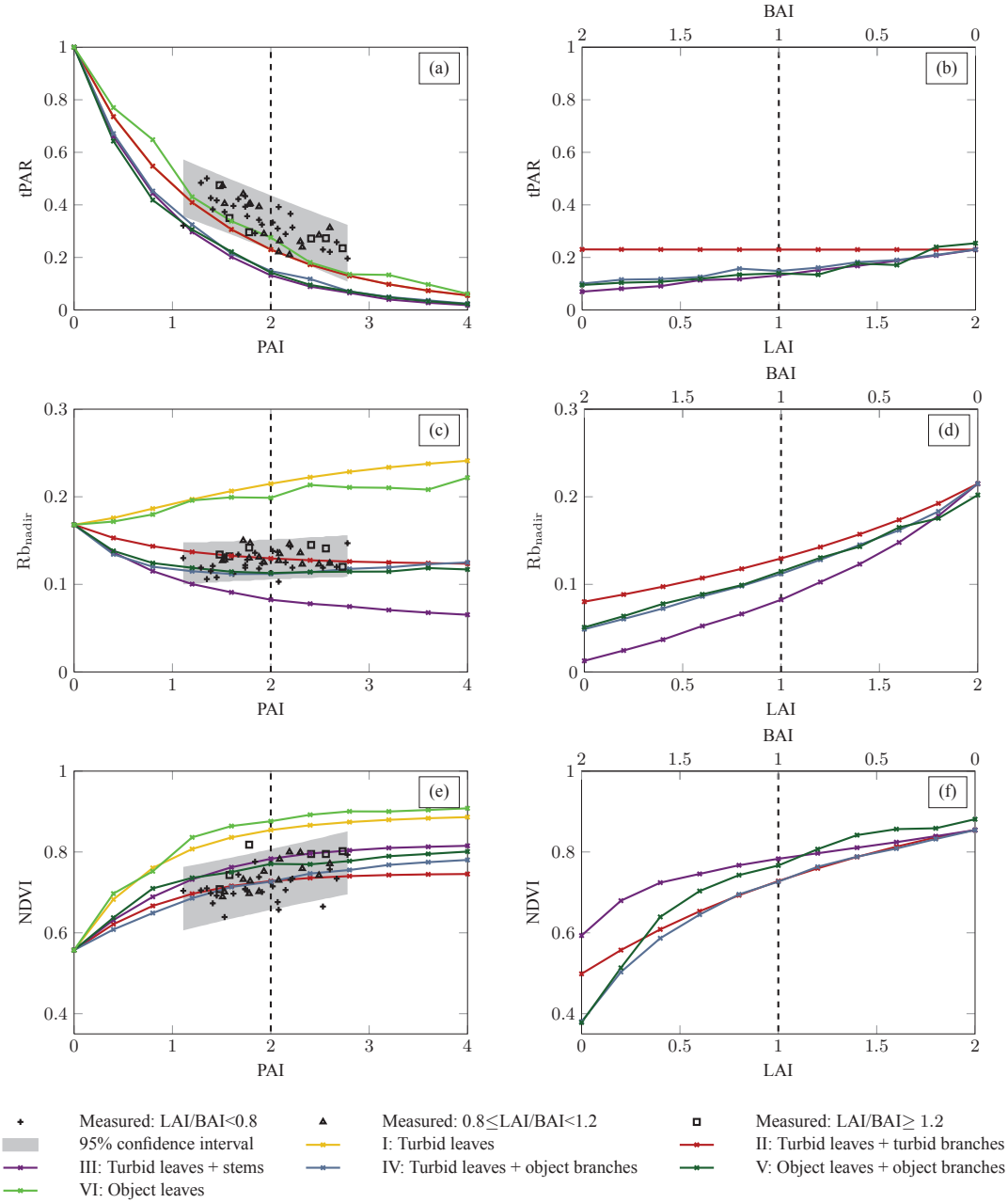

Figure 5: tPAR (top row), Rb_{nadir} (middle row), and NDVI (bottom row) with modelled data using LAI = BAI and measured data from all subplots (left column) and with modelled data using different leaf to branch ratios with PAI = 2 (right column); the different symbols of measured data show three categories of observed leaf / branch ratios; the grey area is the 95% confidence interval around a linear regressions of the data; the vertical dashed lines mark the input parameter set shown in all subplots.

The simulation with stems (III) underestimates the amount of reflected solar radiation, as results show a strong decline in reflectance in the range of modelled PAI (Figure 5, c). Apparently the vertical orientation of the stems is not a good approximation of the dwarf birch shrubs and the effect of shading is overestimated. The differences between simulations which include turbid or object branches (II, IV, and V) are less pronounced and the modelled reflectance is within the 95% confidence interval of measured data. Complexities II, IV, and V show very little variation in reflectance when PAI is in the range of 1-3 PAI. This model result agrees well with our field measurements. If leaves and branches are simulated as turbid media, the reflectance decreases slightly with increasing PAI, a trend observed across the whole range (1-3 PAI). The simulation with turbid leaves and object branches (IV) and leaves and branches as objects (V) show a minimum reflectance at PAI = 1.6 and PAI = 2, respectively, and an increase in reflectance for denser canopies (Figure 5, c). A higher contribution of leaves to the PAI increases the broadband reflectance for all model complexities (Figure 5, d). In general the ratio between leaves and branches has a stronger effect on the modelled reflectance than the total PAI with LAI = BAI.

Apart from broadband nadir reflectance, we also used the spectral reflectance for model validation (Figure 6). Two different spectral regions can be distinguished, the visible and the near infrared range. In the visible range all model complexities show different results, especially at the green peak. The green peak (≈550 nm) is highest in model complexities which include only leaves (I, VI) and lowest with turbid leaves and stems (III) (Figure 6, a). Complexity V (object leaves and branches) also underestimates the green peak in simulations with LAI = BAI. The effect of total PAI on reflectance in the visible is small for PAI > 0.8 (Figure 6, b). However, the ratio between leaves and branches is very important for both the shape of the reflectance spectrum and the absolute values (Figure 6, c). The more leaves are simulated compared to branches, the more pronounced is the reflectance peak in the green and the minimum in the red. Additionally, more leaves result in higher total reflectance in the visible range. The results for LAI > BAI fit the measured data much better than simulations

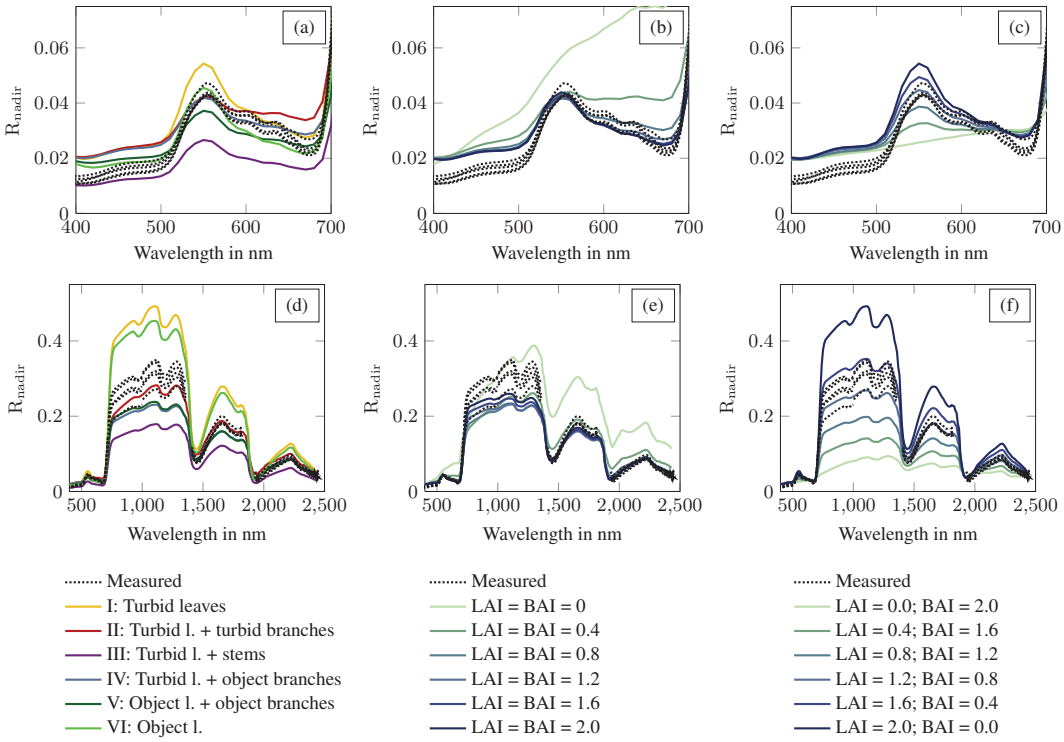

Figure 6: Reflectance in nadir direction (R_{nadir}) in the visible range (top row) and whole range (bottom row) measured on the five control plots 08/07/2013 (PAI between 1.78 and 2.3, Figure 4) in comparison with (a,d) model results for PAI = 2, LAI = BAI, (b,e) model results for different PAIs with turbid leaves and object branches (IV) and (c,f) model results with PAI = 2 and different ratios of LAI/BAI with turbid leaves and object branches (IV); one legend per column.

with less leaves.

In the near infrared the models with only leaves overestimate the reflected radiation drastically. Using LAI = BAI = 1 the model including the vertical stems (III) underestimates the reflectance and the other model complexities are within the range of the control subplot measurements (Figure 6, d). As in the visible part of the spectrum, total PAI is most important for reflectance in the near infrared for PAI < 0.8 (Figure 6, e). The leaf to branch ratio strongly influences the modelled reflectance (Figure 6, f), especially the absolute values.

3.4. NDVI - data and model results

As expected, we found a positive relationship between NDVI and PAI (Figure 5, e). However, NDVI is more strongly correlated with LAI than PAI and is not at all correlated with BAI (Table 3). In general the relationship between NDVI and LAI is much more pronounced than between reflectance and LAI. Our measurements of the background reveal an average NDVI of 0.56 (Figure 4, e), which agrees well with contact measurements of the mosses below the shrubs. The measured NDVIs of dwarf birch canopy range between 0.61 and 0.82 and the lowest NDVI values were measured on plots with lower leaf / branch ratios (Figure 5, e).

All model simulations show an increase of NDVI with PAI, but the complexities differ in the maximum NDVI returned for large PAIs (Figure 5, e). The simulations with only leaves (I and VI) overestimate NDVI strongly, while all simulations which include branch optical properties (II, III, IV, and V) simulate values in the range of the confidence interval. As we found in the model results for reflectance, NDVI simulations are very sensitive to the ratio of leaves to branches (Figure 5, f).

3.5. Energy balance - model results

We used the DART model output to estimate the importance of branches and leaves in the energy balance. Here we only show modelling results for IV (object branches and turbid leaves), however, the results are very similar for V (object branches and object leaves). As described above, the fraction of reflected energy is almost the same for different PAIs (Figure 7, a). The amount of absorbed radiation by the background decreases non-linearly with increasing PAI as leaves and branches provide more and more shading. For LAI = BAI branches contribute between 71% (low PAI) and 57% (high PAI) to the total absorption of the canopy.

The ratio between leaves and branches does not only change the partitioning of absorbed radiation within the vegetation layer, but also the amount of energy

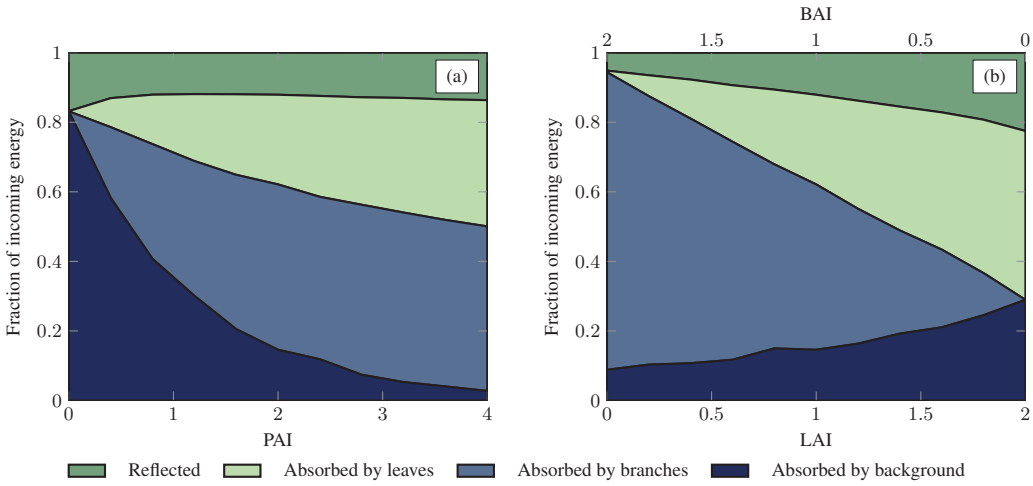

Figure 7: Energy balance as simulated with complexity IV (object branches and turbid leaves) (a) modelled data using LAI = BAI and (b) modelled data using different leaf to branch ratios with PAI = 2.

absorbed by the background (Figure 7, b). A higher fraction of leaves leads to greater reflection and higher absorption by the background layer.

4. Discussion

4.1. Field data

In our study the ratio between leaf and branch area changes during the season from 0.73 on average before treatment to 1.22 as the mean of the control subplots at the last measurement in mid-July. The early-season measurements correspond well to the ratio of 0.7 for tall Arctic shrubs measured by Thompson et al. (2004). It has to be noted that our measurements likely underestimate both LAI and BAI as we used point-quadrat grid measurements with vertical needle insertion.

Our treatments did not affect LAI and BAI equally but rather changed the ratio between the two. This is especially true for the height treatment which cannot be considered representative of a naturally shorter canopy. The treatment removed mostly young branch tips with many leaves while older, more

woody parts of the canopy remained. This combination of changes in PAI and leaf / branch ratio between each treatment is a limitation when comparing the measurements to the model results and when drawing conclusions on natural changes.

Transmitted radiation was underestimated by the radiative transfer model in all complexities. We propose two main reasons. First, the measurements may overestimate tPAR as the sky was overcast on the second and third sampling date. Cloud cover can increase tPAR as diffuse light is expected to reduce shadows (Eck & Deering, 1992; Reid et al., 2014). However, our data does not show a systematic difference between the clear-sky pre-treatment measurements and the two sets of overcast measurements. As such the measurement conditions do not completely explain the differences. The second reason for the differences could lie in the model parameterisation. We did not consider clumping in our model runs with turbid media, and in the object based complexities we may be underestimate leaf and branch clumping.

The values of nadir reflectance between 0.1 and 0.15 measured in our study (Figure 4) are slightly lower than the albedo values reported for dwarf birch dominated tundra in literature, which are 0.16 (Eugster et al., 2000) and 0.17 (Thompson et al., 2004; Beringer et al., 2005). One reason may be that, as shown by our model results for local conditions, nadir reflectance is slightly lower than albedo. Another possibility is that our dataset only includes selected, clear-sky values collected around noon and is therefore not a complete data series. Furthermore we selected specifically dwarf birch patches with closed dwarf birch cover while other studies include larger fractions of other species. In the studies by Thompson et al. (2004) and Beringer et al. (2005) dwarf shrub tundra includes a mixture of vegetation containing dwarf birch as well as other deciduous and evergreen shrubs. The albedo value from Eugster et al. (2000) was measured on a plot with dwarf birch and willow species.

Blok et al. (2011c) found a negative relationship between shrub fractional cover and albedo at the Kytalyk research site on experimental plots in 2009. In contrast, our results show a weak positive correlation between nadir reflectance

and PAI. One reason for this discrepancy might be that we compare different variables. Our study focused on nadir reflectance and LAI, while Blok et al. (2011c) measured albedo and fractional cover. However, our model results show a strong positive correlation between albedo and nadir reflectance and Blok et al. (2011c) report a positive relation between dwarf shrub fractional cover and LAI. Therefore, it is not expected that slightly different variables would lead to the observed change in relationship between plant area proxies and reflectance quantities. Another reason for the discrepancy between the studies may be the difference in observed LAI ranges. In our study LAI varied between 0.36 and 1.48 compared to a range of 0.2 to 1 in Blok et al. (2011c). Our model results show that the initial decrease of nadir reflectance seen with increasing PAI between 0 and 1, levels off for PAI > 1. These results also suggest that reflectance may increase at higher PAI values, especially if the number of leaves as compared to branches increases (IV, Figure 5 c, d). As such both our and Blok et al. (2011c) measurements may be showing different parts of the picture. It is important to note that both studies report a weak correlation with R^2 values of $0.37^2 = 0.14$ (Table 3) and 0.47, respectively. This may be in part due to the relatively few measurements included, especially in the LAI - albedo relationship of Blok et al. (2011c).

Several studies show a negative correlation between biomass or LAI and canopy reflectance across different ecosystem types in the Arctic (e.g. Thompson et al., 2004; Beringer et al., 2005). In contrast our measurements and model results show that for the given shrub vegetation increasing PAI does not significantly decrease the growing season albedo. Thus studies that relate Arctic greening to the radiation balance need to differentiate between greening through increased growth of the existing vegetation type and greening through replacement of one vegetation type with another. In addition, our study focused on the growing season while several studies suggest, that the most important effect of shrub presence and height on the radiation balance is in winter and spring when the shrubs mask the snow and enhance snowmelt (e.g. Pomeroy et al., 2006; Marsh et al., 2010; Loranty et al., 2011).

Our NDVI measurements of dwarf birch canopy range from 0.6 to 0.8 (Figure 5, e). This range agrees well with other studies from shrub tundra (Riedel et al., 2005; Blok et al., 2011c) which also report a positive relationship between NDVI and shrub cover. However, our data and model results indicate a saturation of NDVI for PAIs starting between 2 and 3 (Figure 5, e). Thus NDVI might be less useful for relating further Arctic greening to biomass (Rees et al., 1998), especially as it also relates to other factors like moisture conditions (Gamon et al., 2013) and background type (Hope et al., 1993; Rocha & Shaver, 2009). We found relatively high background NDVI values due to mosses below the shrub canopy. This is consistent with the study by Boelman et al. (2011) which also reports higher NDVI values for vegetation prior to leaf out when woody branch coverage is sparse as compared to more dense branch coverage, which masks the background vegetation.

Our findings have important implications on the summer energy balance of the soil-plant system. Unlike previously thought, a denser shrub canopy may not increase the overall energy availability as the effect on canopy albedo is small and we observed a positive relationship between the two. The major effect of shrub density is on energy partitioning within the canopy-soil system. Denser canopies transmit less radiation to the soil and likely increase energy loss due to evapotranspiration (Bonfils et al., 2012). Therefore, a dense shrub canopy may reduce the ALT and soil temperatures. Furthermore, soil shading influences the plant community below the shrubs as species richness has been found to decline with increasing shrub height and density (Pajunen et al., 2011). More specifically, soil shading has been found to cause reduction in the moss layer below dense shrub canopies which has implications for soil temperatures, active layer depth, and the rate of soil decomposition (Walker et al., 2006; Blok et al., 2011a).

4.2. Simulations

In the past a variety of models, ranging from very simple to 3D Monte Carlo or flux tracking approaches, have been used for simulating radiative transfer in

vegetation. We used the DART model to compare six different 3D approaches. DART proved to be an effective tool for studying the influence of leaf and branch parameterisation in radiative transfer modelling. Our results corroborate other studies which found DART to be a useful tool for modelling radiative transfer in vegetation (Gastellu-Etchegorry et al., 1999, 2004; Malenovský et al., 2008). However, the model had not yet been validated for dwarf-shrub tundra.

The main result of our modelling study is the importance of including branches as well as leaves in radiation balance calculations. The importance of branches, stems or woody elements in general has been stressed by other authors for forest canopies (Malenovský et al., 2008; Verrelst et al., 2010). However, few studies exist on the influence of woody elements on the radiative balance of Arctic shrubs. Two studies that measured transmitted radiation below deciduous Arctic tall-shrub vegetation did so in spring before leaf-out and found significantly reduced radiation compared to open locations (Bewley et al., 2007; Reid et al., 2014). Depending on solar angle and exact measurement location, both studies revealed absorption by the woody biomass of the shrubs to be as much as 60% in extreme cases (low solar angles or dense canopy) and 30 to 40% on average. Our model results suggest, that in dwarf birch vegetation branches are likely to contribute more to total radiation absorption than leaves (Figure 7). As the partitioning changes nonlinearly with PAI, both elements should be included in radiation transfer or energy balance modelling. While PAI is clearly the most important driver for tPAR, the ratio between leaves and branches has a stronger influence on reflectance and NDVI (Figure 5). Thus we would like to emphasise the need for measurements of leaf to branch ratios of different vegetation types so that these ratios can be included in models of the energy or radiation balance.

Four of the six model complexities tested in our study included a parameterisation of branches (II-V). The implementation of branches as vertical stems (III) is not appropriate as it massively underestimates nadir reflectance and is less accurate than branches represented by turbid medium or objects. For the complexities with object branches the differences between leaves as turbid

medium (IV) and as objects (V) are relatively small. These model complexities slightly underestimated nadir reflectance and strongly underestimated tPAR while NDVI is simulated well. The model run with turbid leaves and turbid branches (II) simulates all three variables best although the tPAR values are on the lower boundary of the measurements. It should be noted here, however, that leaf and branch angle distributions are influential parameters for turbid medium calculations and were not measured in the field. Furthermore, we assumed 'no clumping' in our simulations with turbid media because of the lack of input data. Including a clumping factor of 0.8 in the simulation with turbid leaves and branches (II) has a small effect on simulated Albedo and NDVI (less than 3% for all PAI), but increases tPAR significantly by 0.04 to 0.08 depending on the plant area (results not shown). Thus simulations with clumped turbid media match the measured tPAR data best while turbid media without clumping and object branches show strong discrepancies between model results and data. This suggests that also the object branches might be too uniformly distributed on the modelled scene.

It should be noted here that we simulated only one solar angle which corresponds to local conditions one hour before noon. Thus our results for the energy balance (Figure 7) show just a snap-shot and not average values for the whole season.

5. Conclusions

Our most important conclusions concerning Arctic dwarf-shrub vegetation are as follows:

- For plant areas between 1-3 $m^2\,m^{-2}$ nadir reflectance is very weakly correlated with dwarf birch PAI and the relationship is positive.
- Nadir reflectance and NDVI are mainly influenced by leaf area and leaf to branch ratio, less so by plant area.

- Woody biomass of dwarf birch shrubs accounts for 57% to 71% of the total canopy absorbed radiation for LAI = BAI in our model results.

- Energy partitioning between leaves and branches is non linear.

These findings have important implications for the impacts of increased Arctic shrub density. While increasing shrub biomass may not lead to significant albedo reduction under constant ecosystem type, the partitioning of the absorbed radiation between soil and canopy is likely to change. The changes in energy balance of the soil and thus the permafrost may not be easily observable from space as shrub plant area indices above 2 are not significantly related to NDVI or, in general, reflectance in any spectral region.

We demonstrated the importance of leaf to branch ratios for all parts of the shortwave radiation balance. Thus we suggest that more effort is needed to measure this ratio in the field and to explicitly include it in radiative transfer and energy balance models. Furthermore, canopy background and vegetation type replaced by shrubs need to be considered when predicting feedbacks of shrubification to summer albedo, permafrost thaw, and climate warming.

Acknowledgements

We acknowledge the support by ASD Goetz Instrument Support Program for providing a spectrometer for field measurements in the Siberian tundra. We would like to thank the Siberian Branch of the Russian Academy of Science for the support. This work was supported by the Swiss National Science Foundation through project grant 140631. We were further supported by the University of Zurich through the University research priority programme on Global Change and Biodiversity (URPP GCB). We like to thank the developers, especially J.-P. Gastellu-Etchegorry and CESBIO, for making the DART software freely available, and F. Schneider and M. Schaepman at the Remote Sensing Laboratories, University of Zurich, for discussions and comments.

References

Beck, P. S. A., & Goetz, S. J. (2011). Satellite observations of high northern latitude vegetation productivity changes between 1982 and 2008: ecological variability and regional differences. *Environmental Research Letters*, *6*, 045501. doi:10.1088/1748-9326/6/4/045501.

Beringer, J., Chapin III, F. S., Thompson, C. C., & McGuire, A. D. (2005). Surface energy exchanges along a tundra-forest transition and feedbacks to climate. *Agricultural and Forest Meteorology*, *131*, 143–161. doi:10.1016/j.agrformet.2005.05.006.

Berner, L. T., Beck, P. S. A., Bunn, A. G., & Goetz, S. J. (2013). Plant response to climate change along the forest-tundra ecotone in northeastern Siberia. *Global Change Biology*, *19*, 3449–3462. doi:10.1111/gcb.12304.

Bewley, D., Pomeroy, J. W., & Essery, R. L. H. (2007). Solar radiation transfer through a subarctic shrub canopy. *Arctic, Antarctic, and Alpine Research*, *39*, 365–374. doi:10.1657/1523-0430(06-023)[BEWLEY]2.0.CO;2.

Bhatt, U. S., Walker, D. A., Raynolds, M. K., Comiso, J. C., Epstein, H. E., Jia, G., Gens, R., Pinzon, J. E., Tucker, C. J., Tweedie, C. E., & Webber, P. J. (2010). Circumpolar Arctic tundra vegetation change is linked to sea ice decline. *Earth Interactions*, *14*. doi:10.1175/2010EI315.1.

Blok, D., Heijmans, M. M. P. D., Schaepman-Strub, G., Kononov, A. V., Maximov, T. C., & Berendse, F. (2010). Shrub expansion may reduce summer permafrost thaw in Siberian tundra. *Global Change Biology*, *16*, 1296–1305. doi:10.1111/j.1365-2486.2009.02110.x.

Blok, D., Heijmans, M. M. P. D., Schaepman-Strub, G., Ruijven, J. v., Parmentier, F. J. W., Maximov, T. C., & Berendse, F. (2011a). The cooling capacity of mosses: Controls on water and energy fluxes in a Siberian tundra site. *Ecosystems*, *14*, 1055–1065. doi:10.1007/s10021-011-9463-5.

Blok, D., Sass-Klaassen, U., Schaepman-Strub, G., Heijmans, M. M. P. D., Sauren, P., & Berendse, F. (2011b). What are the main climate drivers for shrub growth in Northeastern Siberian tundra? *Biogeosciences*, *8*, 1169–1179. doi:10.5194/bg-8-1169-2011.

Blok, D., Schaepman-Strub, G., Bartholomeus, H., Heijmans, M. M. P. D., Maximov, T. C., & Berendse, F. (2011c). The response of Arctic vegetation to the summer climate: relation between shrub cover, NDVI, surface albedo and temperature. *Environmental Research Letters*, *6*, 035502. doi:10.1088/1748-9326/6/3/035502.

Boelman, N. T., Gough, L., McLaren, J. R., & Greaves, H. (2011). Does NDVI reflect variation in the structural attributes associated with increasing shrub dominance in arctic tundra? *Environmental Research Letters*, *6*, 035501. doi:10.1088/1748-9326/6/3/035501.

Bonfils, C. J. W., Phillips, T. J., Lawrence, D. M., Cameron-Smith, P., Riley, W. J., & Subin, M. (2012). On the influence of shrub height and expansion on northern high latitude climate. *Environmental Research Letters*, *7*, 15503–15511. doi:10.1088/1748-9326/7/1/015503.

Chapin III, F. S., Mcguire, A. D., Randerson, J., Pielke, R., Baldocchi, D., Hobbie, S. E., Roulet, N., Eugster, W., Kasischke, E., Rastetter, E. B., Zimov, S. A., & Running, S. W. (2000). Arctic and boreal ecosystems of western North America as components of the climate system. *Global Change Biology*, *6*, 211–223. doi:10.1046/j.1365-2486.2000.06022.x.

Chapin III, F. S., Sturm, M., Serreze, M. C., McFadden, J. P., Key, J. R., Lloyd, A. H., McGuire, A. D., Rupp, T. S., Lynch, A. H., Schimel, J. P., Beringer, J., Chapman, W. L., Epstein, H. E., Euskirchen, E. S., Hinzman, L. D., Jia, G., Ping, C.-L., Tape, K. D., Thompson, C. D. C., Walker, D. A., & Welker, J. M. (2005). Role of land-surface changes in Arctic summer warming. *Science*, *310*, 657–660. doi:10.1126/science.1117368.

Cowtan, K., & Way, R. G. (2014). Coverage bias in the HadCRUT4 temperature series and its impact on recent temperature trends. *Quarterly Journal of the Royal Meteorological Society*, . doi:10.1002/qj.2297. Accepted Article.

Eck, T. F., & Deering, D. W. (1992). Canopy albedo and transmittance in a spruce-hemlock forest in mid-september. *Agricultural and Forest Meteorology*, *59*, 237–248. doi:10.1016/0168-1923(92)90095-L.

Elmendorf, S. C., Henry, G. H. R., Hollister, R. D., Björk, R. G., Boulanger-Lapointe, N., Cooper, E. J., Cornelissen, J. H. C., Day, T. A., Dorrepaal, E., Elumeeva, T. G., Gill, M., Gould, W. A., Harte, J., Hik, D. S., Hofgaard, A., Johnson, D. R., Johnstone, J. F., Jónsdóttir, I. S., Jorgenson, J. C., Klanderud, K., Klein, J. A., Koh, S., Kudo, G., Lara, M., Lévesque, E., Magnússon, B., May, J. L., Mercado-Díaz, J. A., Michelsen, A., Molau, U., Myers-Smith, I. H., Oberbauer, S. F., Onipchenko, V. G., Rixen, C., Martin Schmidt, N., Shaver, G. R., Spasojevic, M. J., Þ orhallsdóttir, T. o. E., Tolvanen, A., Troxler, T., Tweedie, C. E., Villareal, S., Wahren, C.-H., Walker, X., Webber, P. J., Welker, J. M., & Wipf, S. (2012). Plot-scale evidence of tundra vegetation change and links to recent summer warming. *Nature Climate Change*, *2*, 453–457. doi:10.1038/nclimate1465.

Eugster, W., Rouse, W. R., Pielke Sr, R. A., Mcfadden, J. P., Baldocchi, D. D., Kittel, T. G. F., Chapin III, F. S., Liston, G. E., Vidale, P. L., Vaganov, E., & Chambers, S. (2000). Land–atmosphere energy exchange in Arctic tundra and boreal forest: available data and feedbacks to climate. *Global Change Biology*, *6*, 84–115. doi:10.1046/j.1365-2486.2000.06015.x.

Forbes, B. C., Fauria, M. M., & Zetterberg, P. (2010). Russian Arctic warming and 'greening' are closely tracked by tundra shrub willows. *Global Change Biology*, *16*, 1542–1554. doi:10.1111/j.1365-2486.2009.02047.x.

Gamon, J. A., Huemmrich, K. F., Stone, R. S., & Tweedie, C. E. (2013). Spatial and temporal variation in primary productivity (NDVI) of coastal Alaskan

tundra: Decreased vegetation growth following earlier snowmelt. *Remote Sensing of Environment*, *129*, 144–153. doi:10.1016/j.rse.2012.10.030.

Gastellu-Etchegorry, J.-P., Demarez, V., Pinel, V., & Zagolski, F. (1996). Modeling radiative transfer in heterogeneous 3-D vegetation canopies. *Remote Sensing of Environment*, *58*, 131–156. doi:10.1016/0034-4257(95)00253-7.

Gastellu-Etchegorry, J.-P., Guillevic, P., Zagolski, F., Demarez, V., Trichon, V., Deering, D., & Leroy, M. (1999). Modeling BRF and radiation regime of boreal and tropical forests - I. BRF. *Remote Sensing of Environment*, *68*, 281–316. doi:10.1016/S0034-4257(98)00119-9.

Gastellu-Etchegorry, J.-P., Martin, E., & Gascon, F. (2004). DART: a 3D model for simulating satellite images and studying surface radiation budget. *International Journal of Remote Sensing*, *25*, 73–96. doi:10.1080/0143116031000115166.

Grau, E., & Gastellu-Etchegorry, J.-P. (2013). Radiative transfer modeling in the Earth–Atmosphere system with DART model. *Remote Sensing of Environment*, *139*, 149–170. doi:10.1016/j.rse.2013.07.019.

Hope, A. S., Kimball, J. S., & Stow, D. A. (1993). The relationship between tussock tundra spectral reflectance properties and biomass and vegetation composition. *International Journal of Remote Sensing*, *14*, 1861–1874. doi:10.1080/01431169308954008.

Hope, A. S., Pence, K. R., & Stow, D. A. (2004). NDVI from low altitude aircraft and composited NOAA AVHRR data for scaling Arctic ecosystem fluxes. *International Journal of Remote Sensing*, *25*, 4237–4250. doi:10.1080/01431160310001632710.

Hosgood, B., Jacquemoud, S., Andreoli, G., Verdebout, J., Pedrini, A., & Schmuck, G. (1995, revised 2005). *Leaf Optical Properties EXperiment 93 (LOPEX93)*. Technical Report Report EUR 16095 EN.

Huemmrich, K. F., Gamon, J. A., Tweedie, C. E., Oberbauer, S. F., Kinoshita, G., Houston, S., Kuchy, A., Hollister, R. D., Kwon, H., Mano, M., Harazono, Y., Webber, P. J., & Oechel, W. C. (2010). Remote sensing of tundra gross ecosystem productivity and light use efficiency under varying temperature and moisture conditions. *Remote Sensing of Environment*, *114*, 481–489. doi:10.1016/j.rse.2009.10.003.

Jorgenson, M. T., Romanovsky, V., Harden, J., Shur, Y., O'Donnell, J., Schuur, E. A. G., Kanevskiy, M., & Marchenko, S. (2010). Resilience and vulnerability of permafrost to climate change. *Canadian Journal of Forest Research-revue Canadienne De Recherche Forestiere*, *40*, 1219–1236. doi:10.1139/X10-060.

Kim, Y., Kimball, J. S., Zhang, K., Didan, K., Velicogna, I., & McDonald, K. C. (2014). Attribution of divergent northern vegetation growth responses to lengthening non-frozen seasons using satellite optical-NIR and microwave remote sensing. *International Journal of Remote Sensing*, *35*, 3700–3721. doi:10.1080/01431161.2014.915595.

Loranty, M. M., Goetz, S. J., & Beck, P. S. A. (2011). Tundra vegetation effects on pan-Arctic albedo. *Environmental Research Letters*, *6*, 024014. doi:10.1088/1748-9326/6/2/024014.

Malenovský, Z., Martin, E., Homolová, L., Gastellu-Etchegorry, J.-P., Zurita-Milla, R., Schaepman, M., Pokorný, R., Clevers, J., & Cudlín, P. (2008). Influence of woody elements of a Norway spruce canopy on nadir reflectance simulated by the DART model at very high spatial resolution. *Remote Sensing of Environment*, *112*, 1–18. doi:10.1016/j.rse.2006.02.028.

Marsh, P., Bartlett, P., MacKay, M., Pohl, S., & Lantz, T. (2010). Snowmelt energetics at a shrub tundra site in the western Canadian Arctic. *Hydrological Processes*, *24*, 3603–3620. doi:10.1002/hyp.7786.

Mi, Y., van Huissteden, J., Parmentier, F. J. W., Gallagher, A., Budishchev, A., Berridge, C. T., & Dolman, A. J. (2013). Improving a

plot-scale methane emission model and its performance at a Northeastern Siberian tundra site. *Biogeosciences Discussions*, *10*, 20005–20046. doi:10.5194/bgd-10-20005-2013.

Miller, P. A., & Smith, B. (2012). Modelling tundra vegetation response to recent arctic warming. *AMBIO*, *41*, 281–291. doi:10.1007/s13280-012-0306-1.

Myers-Smith, I. H., Forbes, B. C., Wilmking, M., Hallinger, M., Lantz, T., Blok, D., Tape, K. D., Macias-Fauria, M., Sass-Klaassen, U., Lévesque, E., Boudreau, S., Ropars, P., Hermanutz, L., Trant, A., Collier, L. S., Weijers, S., Rozema, J., Rayback, S. A., Schmidt, N. M., Schaepman-Strub, G., Wipf, S., Rixen, C., Ménard, C. B., Venn, S., Goetz, S., Andreu-Hayles, L., Elmendorf, S., Ravolainen, V., Welker, J., Grogan, P., Epstein, H. E., & Hik, D. S. (2011). Shrub expansion in tundra ecosystems: dynamics, impacts and research priorities. *Environmental Research Letters*, *6*, 045509. doi:10.1088/1748-9326/6/4/045509.

Myers-Smith, I. H., & Hik, D. S. (2013). Shrub canopies influence soil temperatures but not nutrient dynamics: An experimental test of tundra snow–shrub interactions. *Ecology and Evolution*, *3*, 3683–3700. doi:10.1002/ece3.710.

Pajunen, A. M., Oksanen, J., & Virtanen, R. (2011). Impact of shrub canopies on understorey vegetation in western Eurasian tundra. *Journal of Vegetation Science*, *22*, 837–846. doi:10.1111/j.1654-1103.2011.01285.x.

Parmentier, F. J. W., van Huissteden, J., van der Molen, M. K., Schaepman-Strub, G., Karsanaev, S. A., Maximov, T. C., & Dolman, A. J. (2011). Spatial and temporal dynamics in eddy covariance observations of methane fluxes at a tundra site in northeastern Siberia. *Journal of Geophysical Research*, *116*, 3016. doi:10.1029/2010JG001637.

Pearson, R. G., Phillips, S. J., Loranty, M. M., Beck, P. S. A., Damoulas, T., Knight, S. J., & Goetz, S. J. (2013). Shifts in Arctic vegetation and associated

feedbacks under climate change. *Nature Climate Change - Letters*, *3*, 673–677. doi:10.1038/nclimate1858.

Pinty, B., Lavergne, T., Dickinson, R. E., Widlowski, J.-L., Gobron, N., & Verstraete, M. M. (2006). Simplifying the interaction of land surfaces with radiation for relating remote sensing products to climate models. *Journal of Geophysical Research*, *111*, D02116. doi:10.1029/2005JD005952.

Pomeroy, J. W., Bewley, D. S., Essery, R. L. H., Hedstrom, N. R., Link, T., Granger, R. J., Sicart, J. E., Ellis, C. R., & Janowicz, J. R. (2006). Shrub tundra snowmelt. *Hydrological Processes*, *20*, 923–941. doi:10.1002/hyp.6124.

Rees, W. G., Golubeva, E. I., & Williams, M. (1998). Are vegetation indices useful in the Arctic? *Polar Record*, *34*, 333–336. doi:10.1017/S0032247400026036.

Reid, T. D., Essery, R. L. H., Rutter, N., & King, M. (2014). Data-driven modelling of shortwave radiation transfer to snow through boreal birch and conifer canopies. *Hydrological Processes*, *28*, 2987–3007. doi:10.1002/hyp.9849.

Riedel, S. M., Epstein, H. E., & Walker, D. A. (2005). Biotic controls over spectral reflectance of Arctic tundra vegetation. *International Journal of Remote Sensing*, *26*, 2391–2405. doi:10.1080/01431160512331337754.

Rocha, A. V., & Shaver, G. R. (2009). Advantages of a two band EVI calculated from solar and photosynthetically active radiation fluxes. *Agricultural and Forest Meteorology*, *149*, 1560–1563. doi:10.1016/j.agrformet.2009.03.016.

Serreze, M. C., Walsh, J. E., Chapin III, F. S., Osterkamp, T., Dyurgerov, M., Romanovsky, V., Oechel, W. C., Morison, J., Zhang, T., & Barry, R. G. (2000). Observational evidence of recent change in the northern high-latitude environment. *Climatic Change*, *46*, 159–207. doi:10.1023/A:1005504031923.

Solomon, S., Qin, D., Manning, M., Chen, Z., Marquis, M., Averyt, K. B., Tignor, M., & Miller, H. L. (Eds.) (2007). *Climate Change 2007: The Physical Science Basis*. Cambridge University Press.

Sturm, M., Douglas, T., Racine, C., & Liston, G. E. (2005). Changing snow and shrub conditions affect albedo with global implications. *Journal of Geophysical Research*, *110*, G01004. doi:10.1029/2005JG000013.

Sturm, M., Racine, C., & Tape, K. (2001). Climate change: Increasing shrub abundance in the Arctic. *Nature*, *411*, 546–547. doi:10.1038/35079180.

Swann, A. L., Fung, I. Y., Levis, S., Bonan, G. B., & Doney, S. C. (2010). Changes in Arctic vegetation amplify high-latitude warming through the greenhouse effect. *Proceedings of the National Academy of Sciences*, *107*, 1295–1300. doi:10.1073/pnas.0913846107.

Tape, K., Sturm, M., & Racine, C. (2006). The evidence for shrub expansion in Northern Alaska and the Pan-Arctic. *Global Change Biology*, *12*, 686–702. doi:10.1111/j.1365-2486.2006.01128.x.

Thompson, C., Beringer, J., Chapin III, F. S., & McGuire, A. D. (2004). Structural complexity and land-surface energy exchange along a gradient from Arctic tundra to boreal forest. *Journal of Vegetation Science*, *15*, 397–406. doi:10.1111/j.1654-1103.2004.tb02277.x.

van der Molen, M. K., van Huissteden, J., Parmentier, F. J. W., Petrescu, A. M. R., Dolman, A. J., Maximov, T. C., Kononov, A. V., Karsanaev, S. V., & Suzdalov, D. A. (2007). The growing season greenhouse gas balance of a continental tundra site in the Indigirka lowlands, NE Siberia. *Biogeosciences*, *4*, 985–1003. doi:10.5194/bg-4-985-2007.

Verrelst, J., Schaepman, M. E., Malenovský, Z., & Clevers, J. G. P. W. (2010). Effects of woody elements on simulated canopy reflectance: Implications for forest chlorophyll content retrieval. *Remote Sensing of Environment*, *114*, 647–656. doi:10.1016/j.rse.2009.11.004.

Walker, D. A., Raynolds, M. K., Daniëls, F. J. A., Einarsson, E., Elvebakk, A., Gould, W. A., Katenin, A. E., Kholod, S. S., Markon, C. J., Melnikov, E. S., Moskalenko, N. G., Talbot, S. S., Yurtsev, B. A., & The other members of the CAVM Team (2005). The Circumpolar Arctic vegetation map. *Journal of Vegetation Science*, *16*, 267–282. doi:10.1111/j.1654-1103.2005.tb02365.x.

Walker, M. D., Wahren, C. H., Hollister, R. D., Henry, G. H. R., Ahlquist, L. E., Alatalo, J. M., Bret-Harte, M. S., Calef, M. P., Callaghan, T. V., Carroll, A. B., Epstein, H. E., Jónsdóttir, I. S., Klein, J. A., Magnússon, B. o., Molau, U., Oberbauer, S. F., Rewa, S. P., Robinson, C. H., Shaver, G. R., Suding, K. N., Thompson, C. C., Tolvanen, A., Totland, O., Turner, P. L., Tweedie, C. E., Webber, P. J., & Wookey, P. A. (2006). Plant community responses to experimental warming across the tundra biome. *Proceedings of the National Academy of Sciences of the United States of America*, *103*, 1342–1346. doi:10.1073/pnas.0503198103.

Widlowski, J.-L., Pinty, B., Clerici, M., Dai, Y., De Kauwe, M., de Ridder, K., Kallel, A., Kobayashi, H., Lavergne, T., Ni-Meister, W., Olchev, A., Quaife, T., Wang, S., Yang, W., Yang, Y., & Yuan, H. (2011). RAMI4PILPS: An intercomparison of formulations for the partitioning of solar radiation in land surface models. *Journal of Geophysical Research*, *116*, G02019. doi:10.1029/2010JG001511.

List of Figure Captions

1. Overview of the stations location in north-east Siberia and the extent of Arctic tundra (a, dark grey, data from Walker et al. (2005)), satellite image (GeoEye-1) of the site with the location of the five plots (b, red squares), tundra landscape (c) and dwarf birch vegetation (d, detail of about 60·90 cm).
2. Mean dwarf birch leaf (a) and bark optical properties and background reflectance (b).

3. Visualisation of the six DART model complexities, each shown for LAI = BAI = 0.2; III and IV additionally contain leaves as turbid medium which would obstruct the branches in the visualisation.

4. Effect of treatment and variation with time of LAI (a), BAI (b), tPAR (c), Rb_{nadir} (d), and NDVI (e); the central mark of the boxes is the median of five replicate plots, the edges are the 25th and 75th percentiles, and the whiskers denote the most extreme values; significance of the difference between control and other treatment subplots for each time step: $p < 0.001 :^{\star\star\star}, p < 0.01 :^{\star\star}, p < 0.05 :^{\star}$; measurement dates in Table 1.

5. tPAR (top row), Rb_{nadir} (middle row), and NDVI (bottom row) with modelled data using LAI = BAI and measured data from all subplots (left column) and with modelled data using different leaf to branch ratios with PAI = 2 (right column); the different symbols of measured data show three categories of observed leaf / branch ratios; the grey area is the 95% confidence interval around a linear regressions of the data; the vertical dashed lines mark the input parameter set shown in all subplots.

6. Reflectance in nadir direction (R_{nadir}) in the visible range (top row) and whole range (bottom row) measured on the five control plots 08/07/2013 (PAI between 1.78 and 2.3, Figure 4) in comparison with (a,d) model results for PAI = 2, LAI = BAI, (b,e) model results for different PAIs with turbid leaves and object branches (IV) and (c,f) model results with PAI = 2 and different ratios of LAI/BAI with turbid leaves and object branches (IV); one legend per column.

7. Energy balance as simulated with complexity IV (object branches and turbid leaves) (a) modelled data using LAI = BAI and (b) modelled data using different leaf to branch ratios with PAI = 2.